

## Creep analysis of a rotating functionally graded simple blade: steady state analysis

Manouchehr Mohammad Hosseini Mirzaei <sup>a</sup>, Mohammad Arefi\* and Abbas Loghman <sup>b</sup>

*Department of Solid Mechanics, Faculty of Mechanical Engineering, University of Kashan, I.R. Iran*

*(Received May 7, 2019, Revised August 8, 2019, Accepted October 25, 2019)*

**Abstract.** Initial thermo-elastic and steady state creep deformation of a rotating functionally graded simple blade is studied using first-order shear deformation theory. A variable thickness model for cantilever beam has been considered. The blade geometry and loading are defined as functions of length so that one can define his own blade profile and loading using any arbitrary function. The blade is subjected to a transverse distributed load, an inertia body force due to rotation and a distributed temperature field due to a thermal gradient between the tip and the root. All mechanical and thermal properties except Poisson's ratio are assumed to be longitudinally variable based on the volume fraction of reinforcement. The creep behaviour is modelled by Norton's law. Considering creep strains in stress strain relation, Prandtl-Reuss relations, Norton's law and effective stress relation differential equation in term of effective creep strain is established. This differential equation is solved numerically. By effective creep strain, steady state stresses and deflections are obtained. It is concluded that reinforcement particle size and form of distribution of reinforcement has significant effect on the steady state creep behavior of the blade.

**Keywords:** simple blade; functionally graded material; steady state creep; first-order shear deformation theory (FSDT)

### 1. Introduction

Turbine blades are one of the most important and sensitive parts of aircraft engines working under creep condition. These parts are subjected to complicated mechanical and thermal loads. For this reason, they must be checked or replaced at overhaul time. Creep phenomenon is the most important damage mechanism exhausting the life of the blades (Almasi 2015). To cope with the severe thermal and mechanical loading condition, functionally graded materials have been developed by researchers. Ceramics can tolerate high temperature environment while metals are suitable for mechanical load carrying components. Metal matrix composites reinforced by ceramics are the most common FGM materials employing at high temperature and loading condition. Therefore, the use of FGM is the perfect selection for producing turbine blade (Oh and Yoo 2016). The blade stress at constant speed and transient conditions with nonlinear damping has been determined by Rao and Vyas (1996). They used beam theory for simulation of blade. Shi et al. developed an efficient finite element modeling of composite beams and plates using higher-order theories (Shi *et al.* 1998). They found that the present composite beam element is more accurate than the higher-order beam elements. Sankar (2001) obtained an elasticity solution for a functionally

graded beam subjected to transverse loads and supposed that Young's modulus depends on thickness of beam. Base on this paper, Sankar and Tzeng (2002) investigated thermal stresses in functionally graded beams. Chakraborty *et al.* (2003) developed a new beam element for investigating the thermoelastic behavior of functionally graded beam structures. They based it on the first-order shear deformation theory. Kapania and Raciti (1989) presented a review of shear deformation theories used for the static, vibration and buckling analysis of beams and plates. Also they review of various studies on the delamination buckling in beams and plates. Li (2008) presented a new unified approach for analyzing the static and dynamic behaviors of functionally graded beams with the body force and shear deformation. Kadoli *et al.* (2008) investigated static analysis of functionally graded beams using higher order shear deformation theory. They showed distribution of transverse shear stress profile depends on the metal-ceramic combination. A static result presented for a cantilever functionally graded beams and two wave speeds are obtained when using the Timoshenko beam theory. Sapountzakis and Panagos (2008) investigated shear deformation effect on the elastic response of trapezoidal composite beams. They presented numerical procedures based on the analytical method. linear static analysis of FGM beams using classical and axiomatic refined theories is presented (Giunta *et al.* 2010). Material properties are exponentially considered varying along the one or two directions on the cross-section. The comparison of results indicated that presented higher order models are accurate and affordable in term of computational cost than finite element method. Also, thermo-mechanical response of FGM beams based on a unified formulation is investigated

\*Corresponding author, Associate Professor,  
E-mail: arefi63@gmail.com

<sup>a</sup> Ph.D. Student, E-mail: mmhmirzaei@yahoo.com

<sup>b</sup> Professor, E-mail: aloghman@kashanu.ac.ir

(Giunta *et al.* 2013) and results obtained are validated with finite element analysis, as in the previous article.

Kiani and Eslami (2010) presented formulations for Buckling of beams made of functionally graded material under various types of thermal and boundary conditions. thermoelastic behavior of simply supported variable thickness beams is presented by Xu and Zhou (2012). Nguyen *et al.* (2013) developed static and free vibration of axially loaded functionally graded beams based on the first-order shear deformation theory. They found that their model is efficient in analyzing static and free vibration problem of FG beams. Duy *et al.* (2014) studied free vibration of FGM variable thickness beam resting on elastic supports. They assume material properties are variable Transversely. Niknam *et al.* (2014) studied Non-linear bending analysis of tapered functionally graded (FG) beam subjected to thermal and mechanical load with general boundary condition. In this article, in the case of no axial force along the beam a close form solution is presented but for the general case with axial force, the Galerkin technique is employed. Static analysis of functionally graded material beam performs based on the 1D Carrera Unified Formulation (CUF) and results are compared with various theories (E.g. Euler-Bernoulli Beam Theory (EBBT), First-order Shear Deformation Theory (FSDT)) and finite elements (Filippi *et al.* 2015). Also 1D Carrera Unified Formulation (CUF) is employed in the analysis of thin-walled composite tapered structures (Zappino *et al.* 2018). Oh and Yoo (2016) presented a new method for vibration analysis of rotating pretwisted tapered blades made of functionally graded materials. They investigated effects of the volume fraction index, Young's modulus ratio, hub radius ratio, pretwist angle, taper ratios, width-to-thickness ratio and angular speed upon the dimensionless natural frequencies of the FG blade. Hamdia *et al.* (2018) presented sensitivity and uncertainty analysis for flexoelectric cantilever nanobeams. They performed this analysis for Pure and composite beam. For more information about sensitivity and uncertainty analysis, please refer to (Vu-Bac *et al.* 2016, Hamdia *et al.* 2017). Roy and Meguid (2018) modeled the turbine blade as a tapered Timoshenko beam. They presented effect of the slenderness ratio on the both lateral and axial natural frequencies.

Arefi *et al.* (2016) presented two-dimensional thermoelastic analysis of a functionally graded cylindrical pressure vessel subjected to axially variable thermal and mechanical loads using the First-order shear deformation theory. The obtained results indicated that the boundary conditions of the cylinder have significant effect on thermoelastic response of the vessel. Arefi and Zenkour (2017a) presented the governing equations of motion for a sandwich curved beam including an elastic core and two piezo-magnetic face-sheets using the First-order shear deformation theory. They studied the influence of important parameters of the presented model on the electro-mechanical responses of the problem. In another article they derived the governing equations of bending analysis of a sandwich microbeam using higher-order sinusoidal shear deformation beam theory (Arefi and Zenkour 2017b). The sandwich microbeam includes an elastic micro-core and

two piezoelectric micro face-sheets. They showed that various types of parameters such as foundation, material and loads parameters have significant effect on the bending results.

Loghman and Wahab (1996) investigated creep stresses, strains and damages of thick-walled tubes subjected to an internal pressure and a thermal gradient by using the  $\epsilon$  projection concept. They described a numerical model developed for the computation of creep damages in a thick-walled tube. Base on this research and (Kordkheili and Naghdabadi 2007). Loghman *et al.* investigated time-dependent creep stress redistribution analysis of thick-walled FGM spheres (Loghman *et al.* 2011) and rotating cylinder made of Al-SiC composite (Loghman *et al.* 2017b). Time-dependent creep behavior of FGM hollow spheres has been investigated by Jafari Fesharaki *et al.* (2014). In this work the influence of inhomogeneity on creep response has been reported. Golmakaniyoon and Akhlaghi (2016) studied time-dependent thermoelastic creep behavior of functionally graded beams made of Al-SiC under in-plane thermal loading. The only loading is a distributed temperature field due to steady-state heat conduction from bottom to top surface of the beam. Loghman *et al.* presented time-dependent creep analysis of a thick wall FGM cylinder by using first order shear deformation theory (FSDT) (Loghman *et al.* 2017a). Impact of non-homogeneous index of functionally graded materials on the behaviors of the cylinder was investigated. A semi-analytical method for creep analysis of homogeneous thick truncated conical shells made of 304L austenitic stainless steel based on the first order shear deformation theory (FSDT) presented by Davoudi Kashkoli and Zamani Nejad (Davoudi Kashkoli and Nejad 2018). They predicted time to rupture and remaining life assessment by Larson-Miller Parameter (LMP) and Robinson's linear life fraction damage rule.

In all of these literatures, the material properties of FG beams are assumed to vary continuously through the beam thickness while we have considered longitudinal variable properties. A common and applicable method for analysis of complex parts (such as turbine blades) is computational methods (Anitescu *et al.* 2019).

In this research, the blade is thick. If the thickness of blade is thin, we can use (Chau-Dinh *et al.* 2012, Guo *et al.* 2019).

Based on best author's knowledge, although some important works regarding common structures made of functionally graded materials were published, however no comprehensive research on steady state creep analysis of variable thickness blade made of functionally graded materials can be observed in the literature. In this study, not only the material properties are variable longitudinally but also the rotating blade geometry is varying functionally along the blade. Also, a simple formulation presented for steady state creep analysis of an FGM simple blade.

In this paper steady state creep behavior of a FGM turbine blade simplified as a variable thickness rotating cantilever beam, has been studied using Norton's law. The effect of ceramic particle size and arrangement of reinforcement distribution on steady state creep behavior of the blade is investigated. Three different arrangements for

reinforcement particle distribution are considered. Initial elastic and steady state stresses for these three cases are reported. The minimum effective stress distribution which belongs to one of the cases is selected for studying the effect of reinforcement particle size.

## 2. Geometry and loading condition, material properties, and creep constitutive model

A variable thickness blade with a root thickness of  $t_r$  and tip thickness  $t_t$  is considered. The profile of upper and lower surfaces as functions of variable  $x$  in millimeters is  $14e^{-0.01x} + \frac{x}{30}$  and  $-14e^{-0.01x} - \frac{x}{30}$  respectively. Variable transverse mechanical load, centrifugal body force and a distributed thermal field are applied on the blade. The boundary condition at the root of the blade is assumed to be fixed and the tip of the blade is assumed free. The blade is rotating with a constant angular velocity  $\omega = 6000\text{rpm}$ . The transverse variable pressure on the blade is mathematically represented as:  $P(x) = (-0.04(x/L)^2 - 0.03x/L - 0.01)$  MPa which is due to aerodynamic forces acting on the top surface of the blade. The other parameters of the problem are assumed as:  $T_{\text{root}} = 500^\circ\text{K}$ ,  $T_{\text{tip}} = 1100^\circ\text{K}$ ,  $r_0 = 300$  mm. The geometry and loading conditions are shown in Fig. 1. The geometry of the turbine blade is really complex and the closed form solution for thermoelastic and creep behavior of the blade cannot be obtained. However, such a simple model can just show the trend of deformations in a blade.

The reinforcement is linearly distributed in longitudinal direction based on the volume fraction content.

$$VP(x) = V_{\text{root}} + \frac{x}{L} \times (V_{\text{tip}} - V_{\text{root}}) \quad (1)$$

Where variable  $x$  is the coordinate along the blade length and  $L$  is the length of the blade,  $V_{\text{root}}$  and  $V_{\text{tip}}$  are volume fraction of reinforcement at the root and tip of the blade, respectively. In the present work, all properties except Poisson's ratio are considered to be variable in longitudinal direction based on volume percent of reinforcement

$$P(x) = P_{\text{matrix}} + (P_{\text{reinforcement}} - P_{\text{matrix}}) \times \frac{VP(x)}{100} \quad (2)$$

In which  $P(x)$  is represented as a general property.  $P_{\text{matrix}}$  is matrix property,  $P_{\text{reinforcement}}$  is pure reinforcement property, and  $VP(x)$  is volume fraction of reinforcement

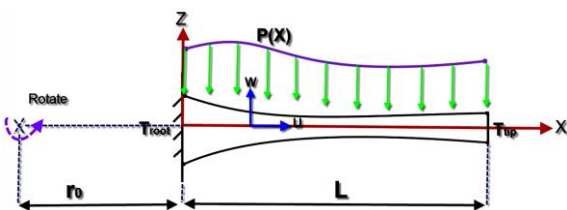


Fig. 1 Sketch of the blade under loading

at position  $x$ . In accordance with Eq. (2), any longitudinal-dependent properties such as elasticity modulus  $E(x)$ , shear modulus  $G(x)$ , thermal conductivity  $K(x)$ , density  $\rho(x)$  and coefficients of heat expansion  $\alpha(x)$  are written as follows

$$\begin{aligned} E(x) &= E_{\text{matrix}} + (E_{\text{reinforcement}} - E_{\text{matrix}}) \times \frac{VP(x)}{100} \\ G(x) &= G_{\text{matrix}} + (G_{\text{reinforcement}} - G_{\text{matrix}}) \times \frac{VP(x)}{100} \\ K(x) &= K_{\text{matrix}} + (K_{\text{reinforcement}} - K_{\text{matrix}}) \times \frac{VP(x)}{100} \\ \alpha(x) &= \alpha_{\text{matrix}} + (\alpha_{\text{reinforcement}} - \alpha_{\text{matrix}}) \times \frac{VP(x)}{100} \\ \rho(x) &= \rho_{\text{matrix}} + (\rho_{\text{matrix}} + \rho_{\text{reinforcement}}) \times \frac{VP(x)}{100} \end{aligned} \quad (3)$$

The following data for matrix and reinforcement properties are used in this investigation (Gupta *et al.* 2004). Where

$$\begin{aligned} E_{Al} &= 70\text{Gpa} \\ E_{SiC} &= 410\text{Gpa} \\ G_{Al} &= 27\text{Gpa} \\ G_{SiC} &= 41.5\text{Gpa} \\ \alpha_{Al} &= 23.1 \times 10^{-6} K^{-1} \\ \alpha_{SiC} &= 4 \times 10^{-6} K^{-1} \\ \rho_{Al} &= 2700\text{kgm}^{-3} \\ \rho_{SiC} &= 3200\text{kgm}^{-3} \\ K_{Al} &= 237\text{Wm}^{-1}C^{-1} \\ K_{SiC} &= 120\text{Wm}^{-1}C^{-1} \end{aligned} \quad (4)$$

Fig. 2 shows three longitudinal distributions of reinforcement used in this study.

These are (A) pure matrix at the root of blade and 30% reinforcement at the tip of blade, (B) matrix with 30% reinforcement at root of blade and pure matrix at tip of blade and (C) pure matrix.

The constitutive relation for creep behavior of materials is represented by Norton's law as follows

$$\dot{\epsilon}_c = B(x)\sigma_e^{n(x)} \quad (5)$$

where  $\dot{\epsilon}_c$  is effective creep strain rate and  $\sigma_e$  is the effective stress. The creep parameters  $B(x)$  and  $n(x)$  are

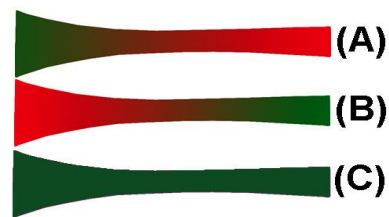


Fig. 2 Longitudinal cross section of the blade for three different composition cases of A, B and C

taken from reference (Gupta *et al.* 2004).

$$\begin{aligned}
 B(x) &= 10^{722.0601911} \times T(x)^{-274.71} \\
 &\quad \times d(x)^{-1.98} \times VP(x)^{-15.88} \\
 n(x) &= 10^{-9.354703141} \times T(x)^{3.80} \\
 &\quad \times d(x)^{0.07} \times VP(x)^{0.07}
 \end{aligned}
 \tag{6}$$

In this relations,  $d(x)$  is the particle size in  $\mu\text{m}$ ,  $T(x)$  is the temperature distribution and  $VP(x)$  is volume fraction of SiC particle at position  $x$ .

### 3. Heat conduction problem

In steady-state heat conduction without any heat generation the Fourier law in longitudinal direction of the blade is considered. According to this, the Fourier law of thermal conductivity can be written as

$$\frac{1}{x} \frac{d}{dx} (xK(x)) \frac{d}{dx} (T(x)) = 0
 \tag{7}$$

It is supposed that the lower and upper surfaces of the cantilever beam are insulated and there is no heat loss. Coefficients of this differential equation are variable. Because of longitudinal-dependent of coefficients, a semi analytical method (Kordkheili and Naghdabadi 2007) to simplify the differential equation has been used. In this method, the cross section of the FGM blade in the  $x$ -direction is divided into a certain number of divisions. The schematic of divisions along the blade length is depicted in Fig. 3.

The coefficients of second-order ordinary differential equation (SODE) are calculated at  $x(k)$  midpoint of each division and the differential equation becomes an ordinary differential equation with constant coefficient. For  $k$ th division the equation is rewritten as

$$\left( \frac{d^2}{dx^2} + S^{(k)} \frac{d}{dx} \right) T = 0
 \tag{8}$$

where

$$\begin{aligned}
 S^{(k)} &= \frac{1}{x^{(k)}} + \frac{1}{K(x^{(k)})} \left. \frac{dK(x)}{dx} \right|_{x=x^{(k)}} \\
 K &= 1, 2, 3, \dots, m
 \end{aligned}
 \tag{9}$$

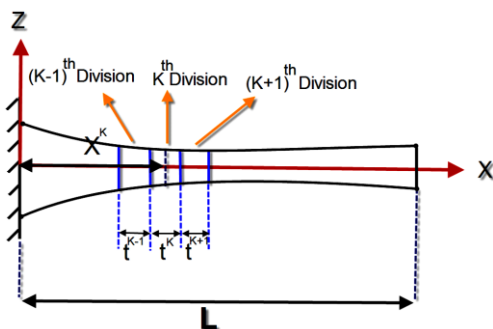


Fig. 3 Division of the blade into a finite number of sub-domains

The SODE with variable coefficients is turn into SODE with constant coefficients for each section. The solution of mentioned SODEs is exactly expressed as

$$T(x^{(k)}) = \bar{R}_1^{(k)} \bar{R}_2^{(k)} \exp(x^{(k)} S^{(k)})
 \tag{10}$$

where  $\bar{R}_1^{(k)}$  and  $\bar{R}_2^{(k)}$  are unknowns constants for  $k$ th sub-domain. These constants are computed using the continuity condition at the interfaces of the adjacent sub-domains. These continuity conditions at the interfaces are written as

$$\begin{aligned}
 T(x) \Big|_{x=x^k + \frac{t^k}{2}} &= T(x) \Big|_{x=x^{k+1} - \frac{t^{k+1}}{2}} \\
 \frac{dT(x)}{dx} \Big|_{x=x^k + \frac{t^k}{2}} &= \frac{dT(x)}{dx} \Big|_{x=x^{k+1} - \frac{t^{k+1}}{2}}
 \end{aligned}
 \tag{11}$$

The global boundary conditions on root and tip surfaces of the FGM blade are

$$\begin{aligned}
 T(x_{root}) &= T_{root} \\
 T(x_{tip}) &= T_{tip}
 \end{aligned}
 \tag{12}$$

Eq. (11) together with Eq. (12) constructs a set of linear algebraic equations with regard to  $\bar{R}_1^{(k)}$  and  $\bar{R}_2^{(k)}$  coefficients. Solving these equations with respect to  $\bar{R}_1^{(k)}$  and  $\bar{R}_2^{(k)}$ , temperature distribution  $T(x)$  can be achieved in each  $x$  division.

### 4. Formulation of the thermoelastic creep analysis

#### 4.1 Thermo-elastic analysis based on FSĐT

In this section, FSĐT is implemented to describe the displacement field of the beam in terms of deformation of mid-surface and rotation about outward axis of the mid-surface (Mirsky 1959). By using this theory, the longitudinal and transverse deformation components are expressed by combination of displacement and rotation components as follows (Arefi *et al.* 2012)

$$\begin{aligned}
 u(x, z) &= u_0 + z\psi(x) \\
 w(x, z) &= w_0
 \end{aligned}
 \tag{13}$$

Where  $u$  and  $w$  are longitudinal and transverse displacement respectively and  $u_0$  shows the longitudinal displacement of the neutral axis,  $w_0$  represents the transverse displacement of the neutral axis in the thickness direction and  $\psi(x)$  is rotation component. By the linear strain–displacement relations, normal and shear strain components are derived as

$$\begin{aligned}
 \epsilon_{xx} &= \frac{\partial u}{\partial x} = \frac{\partial u_0}{\partial x} + z \frac{\partial \psi(x)}{\partial x} + \alpha T(x) \\
 \gamma_{xz} &= \frac{\partial u}{\partial z} + \frac{\partial w}{\partial x} = \psi(x) + \frac{\partial w_0}{\partial x}
 \end{aligned}
 \tag{14}$$

Where  $\epsilon_{xx}$  is the normal strain in longitudinal direction and  $\gamma_{xz}$  is the shearing strain in xz plane. Generalized Hooke's law by considering the thermal strains is written as

$$\begin{aligned} \sigma_{xx} &= E\epsilon_{xx} = E \left[ \frac{\partial u_0}{\partial x} + z \frac{\partial \psi(x)}{\partial x} + \alpha T(x) \right] \\ \tau_{xz} &= G\gamma_{xz} = G \left[ \psi(x) + \frac{\partial w_0}{\partial x} \right] \end{aligned} \quad (15)$$

Where  $\sigma_{xx}$  and  $\tau_{xz}$  are normal and shear stress in xz plane. Substituting the strain components from Eq. (3) into the strain energy density equation and integrating over the volume of the structure, the total strain energy of the beam is obtained. The variation of the strain energy in accordance with the principle of virtual work is

$$\begin{aligned} \delta U &= \int_A \int_Z (\sigma_{xx} \delta \epsilon_{xx} + \tau_{xz} \delta \gamma_{xz}) dz dA = \\ &= \int_A \int_Z \left( \sigma_{xx} \left( \frac{\partial \delta u_0}{\partial x} + z \frac{\partial \delta \psi(x)}{\partial x} + \delta \alpha T(x) \right) + \tau_{xz} \left( \delta \psi(x) + \frac{\partial \delta w_0}{\partial x} \right) \right) dz dA \\ &= \int_A \left( N_{xx} \frac{\partial \delta u_0}{\partial x} + M_{xx} \frac{\partial \delta \psi(x)}{\partial x} + N_{xz} \delta \psi(x) + N_{xz} \frac{\partial \delta w_0}{\partial x} \right) dA \end{aligned} \quad (16)$$

Where  $N_{xx}$ ,  $M_{xx}$  and  $N_{xz}$  are the force and moment per unit length defined as follows

$$\begin{aligned} N_{xx} &= \int \sigma_{xx} dz = \left[ \int E(x) dz \right] \frac{\partial u_0}{\partial x} + \left[ \int z E(x) dz \right] \frac{\partial \psi}{\partial x} \\ &\quad + \int E(x) \alpha(x) T(x) dz \\ N_{xz} &= \int \tau_{xz} dz = \left[ \int G(x) dz \right] \left[ \psi(x) + \frac{\partial w_0}{\partial x} \right] \\ M_{xx} &= \int z \sigma_{xx} dz = \left[ \int z E(x) dz \right] \frac{\partial u_0}{\partial x} \\ &\quad + \left[ \int z^2 E(x) dz \right] \frac{\partial \psi}{\partial x} \\ &\quad + \int E(x) \alpha(x) T(x) z dz \end{aligned} \quad (17)$$

The external work is represented by

$$W = - \int_z F_1(x)u + F_2(x)\psi + F_3(x)w dx \quad (18)$$

Where W is the total external work,  $F_1(x)$  is the centrifugal inertia body force,  $F_2(x)$  is the external torque and  $F_3(x)$  is the transverse load. The load matrix is written as

$$F(x) = \begin{bmatrix} F_1(x) \\ F_2(x) \\ F_3(x) \end{bmatrix} = \begin{bmatrix} \omega^2 \rho(x) h(x) [r_0 + x] \\ 0 \\ -P(x) \end{bmatrix} \quad (19)$$

According to Eq. (18), variation of external work is expressed as

$$\delta W = - \int_z F_1(x)\delta u + F_2(x)\delta \psi + F_3(x)\delta w dx \quad (20)$$

Based on the principle of virtual work, the strain energy variations are equal to the variation of external work, namely (Arefi and Zenkour 2018a, b, c, Arefi *et al.* 2018, Arefi and Zenkour 2017c)

$$\delta U = \delta W \quad (21)$$

The following relationships are obtained according to (16) and the use of the variation calculus.

$$\frac{\partial N_{xx}}{\partial x} + A_5(x)T(x) = F_1(x) - \frac{\partial M_{xx}}{\partial x} + N_{xz} = 0 \quad (22)$$

$$\frac{\partial N_{xz}}{\partial x} + A_6(x)T(x) = F_3(x)$$

By substituting from relation (17) into Eq. (22) the following constitutive differential equations of the problem are obtained.

$$\begin{aligned} A_1(x)u_{,xx} + A_2(x)\psi_{,xx} + A_5(x)T(x) \\ = F_1(x) - A_2(x)u_{,xx}(x) - A_4(x)\psi_{,xx}(x) \\ + A_3(x)\psi(x) + A_3(x)w_{,x}(x) = 0 \end{aligned} \quad (23)$$

$$A_3(x)\psi_{,x}(x) + A_3(x)w_{,xx}(x) + A_6(x)T(x) = F_3(x)$$

Where

$$\begin{aligned} A_1(x) &= \int_{-h(x)/2}^{h(x)/2} E(x) dz \\ A_2(x) &= \int_{-h(x)/2}^{h(x)/2} z E(x) dz \\ A_3(x) &= \int_{-h(x)/2}^{h(x)/2} G(x) dz \\ A_4(x) &= \int_{-h(x)/2}^{h(x)/2} z^2 E(x) dz \\ A_5(x) &= \int_{-h(x)/2}^{h(x)/2} E(x) \alpha(x) dz \\ A_6(x) &= \int_{-h(x)/2}^{h(x)/2} E(x) \alpha(x) z dz \end{aligned} \quad (24)$$

To solve these differential equations with variable coefficients a semi analytical division method has been used (Kordkheili and Naghdabadi 2007).

A large number are divisions in longitudinal direction are considered. For the center point of each division, the Eq. (23) are solved and, using the local boundary conditions introduced in relations (25), and global boundary condition (26), a set of algebraic equation containing constant coefficients of each division are obtained. Solving these equations constants are obtained, then displacements, stresses and strains are achieved.

The local boundary conditions that are due to the continuity condition are

$$\begin{aligned}
 u\left(x^k + \frac{t^k}{2}\right) &= u\left(x^{k+1} - \frac{t^{k+1}}{2}\right) \\
 \psi\left(x^k + \frac{t^k}{2}\right) &= \psi\left(x^{k+1} - \frac{t^{k+1}}{2}\right) \\
 w\left(x^k + \frac{t^k}{2}\right) &= w\left(x^{k+1} - \frac{t^{k+1}}{2}\right) \\
 u_{,x}\left(x^k + \frac{t^k}{2}\right) &= u_{,x}\left(x^{k+1} - \frac{t^{k+1}}{2}\right) \\
 \psi_{,x}\left(x^k + \frac{t^k}{2}\right) &= \psi_{,x}\left(x^{k+1} - \frac{t^{k+1}}{2}\right) \\
 w_{,x}\left(x^k + \frac{t^k}{2}\right) &= w_{,x}\left(x^{k+1} - \frac{t^{k+1}}{2}\right)
 \end{aligned}
 \tag{25}$$

And the root and tip boundary conditions of the cantilever FGM blade are

$$\begin{aligned}
 B. c. : & \begin{cases} u = 0 \\ \psi = 0 \quad x = 0 \\ w = 0 \end{cases} \\
 B. c. : & \begin{cases} N_{xz} = \int \tau(x, z) dA = 0 \\ M_{xx} = \int z \sigma_{xx} dA = 0 \quad x = 0 \\ N_{xx} = \int \sigma_{xx} dA = 0 \end{cases}
 \end{aligned}
 \tag{26}$$

According to the division method, Eq. (23) for Kth division is rewritten as follows

$$\begin{aligned}
 & A_1(x^k)u_{,xx}(x^k) + A_2(x^k)\psi_{,xx} + A_5(x^k)T(x^k) \\
 & = F_1(x^k) - A_2(x^k)u_{,xx}(x^k) - A_4(x^k)\psi_{,xx}(x^k) \\
 & + A_3(x^k)\psi(x^k) + A_3(x^k)w_{,x}(x^k) = 0
 \end{aligned}
 \tag{27}$$

$$\begin{aligned}
 & A_3(x^k)\psi_{,x}(x^k) + A_3(x^k)w_{,xx}(x^k) + A_6(x^k)T(x^k) \\
 & = F_3(x^k)
 \end{aligned}$$

Where

$$\begin{aligned}
 A_1(x^k) &= \int_{-h(x^k)/2}^{h(x^k)/2} E(x^k) dz \\
 A_2(x^k) &= \int_{-h(x^k)/2}^{h(x^k)/2} z E(x^k) dz \\
 A_3(x^k) &= \int_{-h(x^k)/2}^{h(x^k)/2} G(x^k) dz \\
 A_4(x^k) &= \int_{-h(x^k)/2}^{h(x^k)/2} z^2 E(x^k) dz \\
 A_5(x^k) &= \int_{-h(x^k)/2}^{h(x^k)/2} E(x^k) \alpha(x^k) dz \\
 A_6(x^k) &= \int_{-h(x^k)/2}^{h(x^k)/2} E(x^k) \alpha(x^k) z dz
 \end{aligned}
 \tag{28}$$

### 4.2 Steady-state creep analysis

For steady state creep analysis, creep strains are included into the stress-strain relations. Total strain is the

sum of elastic, thermal, and creep strains which can be written

$$\begin{aligned}
 \sigma_{xx} &= \frac{E}{(1+\nu)(1-2\nu)} \left[ (1-\nu)\epsilon_{xx} \right] + \nu(\epsilon_{yy} + \epsilon_{zz}) - \frac{E}{1-2\nu} \alpha T \\
 &\quad - \frac{E}{(1+\nu)(1-2\nu)} \left[ \epsilon_{xx}^c + \nu(\epsilon_{yy}^c + \epsilon_{zz}^c) \right]
 \end{aligned}
 \tag{29}$$

$$\tau_{xz} = \tau_{xz}^{elastic} - 2G \epsilon_{xz}^c$$

where  $\epsilon_{xx}^c$ ,  $\epsilon_{yy}^c$  and  $\epsilon_{zz}^c$  are creep strains along x, y and z direction respectively and  $\epsilon_{xz}^c$  is creep strain in x-z plane. Creep strains are depending on time, temperature and stress. According to the Prandtl-Reuss relations, creep strain increments are related to the current stresses and the material uni-axial creep behavior (Mendelson 1968) as follows

$$\begin{aligned}
 \dot{\epsilon}_{xx}^c &= \frac{\dot{\epsilon}_e^c}{\sigma_e} (\sigma_{xx}) \\
 \dot{\epsilon}_{zz}^c &= \frac{\dot{\epsilon}_e^c}{2\sigma_e} (-\sigma_{xx}) \\
 \dot{\epsilon}_{yy}^c &= -\dot{\epsilon}_{xx}^c - \dot{\epsilon}_{zz}^c \\
 \dot{\epsilon}_{xz}^c &= \frac{3\dot{\epsilon}_e^c}{2\sigma_e} (\tau_{xz})
 \end{aligned}
 \tag{30}$$

Differentiating Eq. (29) with respect to time gives stresses rate.

$$\begin{aligned}
 \dot{\sigma}_{xx} &= \frac{E(\nu-1)}{(1+\nu)(1-2\nu)} (\dot{\epsilon}_{xx}^c) \\
 \dot{\tau}_{xz} &= -2G \dot{\epsilon}_{xz}^c
 \end{aligned}
 \tag{31}$$

Substituting Eqs. (5) and (30) into Eq. (31) and integrating stresses are obtained in terms of effective creep strain as follows

$$\begin{aligned}
 \sigma_{xx} &= e^{\left( \frac{E(\nu-1)n(x)}{(1+\nu)(1-2\nu)(2n(x)-1)} B(x) \frac{1}{n(x)} \epsilon_e^c \left( \frac{2n(x)-1}{n(x)} \right) \right)} + c_1 \\
 \tau_{xz} &= e^{-3G B(x) \frac{1}{n(x)} \frac{n(x)}{2n(x)-1} \epsilon_e^c \left( \frac{2n(x)-1}{n(x)} \right)} + c_2
 \end{aligned}
 \tag{32}$$

Constant coefficients C1 and C2 are obtained continuity conditions at the border of divisions.

$$\begin{aligned}
 \sigma_{xx}\left(x^k + \frac{t^k}{2}\right) &= \sigma_{xx}\left(x^{k+1} - \frac{t^{k+1}}{2}\right) \\
 \tau_{xz}\left(x^k + \frac{t^k}{2}\right) &= \tau_{xz}\left(x^{k+1} - \frac{t^{k+1}}{2}\right)
 \end{aligned}
 \tag{33}$$

Von Mises equivalent or effective stress are derived as follows

$$\sigma_e = \sqrt{\sigma_{xx}^2 + 3\tau_{xz}^2}
 \tag{34}$$

Effective creep strain rate is obtained substituting Eq. (34) into constitutive Eq. (5) as follows

$$\begin{aligned}
 \dot{\epsilon}_e^c &= B(x^k) \\
 & \left( \left( e^{-\frac{E(x^k)(1+\nu)n(x^k)}{(1+\nu)(1-2\nu)(2n(x^k)-1)} B(x^k) \frac{1}{n(x^k)} \epsilon_e^c \left( \frac{2n(x^k)-1}{n(x^k)} \right)} \right) + C_1 \right)^2
 \end{aligned}
 \tag{35}$$

$$+3(e^{-3G(x^k)B(x^k)n(x^k)} \frac{1}{2n(x^k)-1} \frac{n(x^k)}{e^{\frac{(2n(x^k)-1)}{n(x^k)}}} + C_2)^2)^{\frac{n(x^k)}{2}} \quad (24)$$

The effective creep strain rate of steady state condition at all division points are obtained from numerical solution of Eq. (35). Steady state stresses are then calculated from Eq. (32).

### 5. Numerical results and discussion

In this section, the numerical results and corresponding conclusions are presented. This section is including the initial thermoelastic results and steady state creep stresses and displacements. The particle size at this stage is  $d = 1.7 \mu\text{m}$ .

An important ingredient of thermoelastic analysis is the temperature distribution field. Three different cases of temperature distribution due to three different volume content distribution (A, B, C) of reinforcement are calculated and plotted in Fig. 4. This figure indicated that composite blade of case (B) has the minimum temperature distribution throughout the longitudinal direction of the blade. In general, effect of reinforcement particles on temperature distribution of the blade is not really significant.

Initial elastic and final steady state creep longitudinal displacement for three different cases A, B and C are shown in Fig 5. The boundary condition of fixed root and free tip

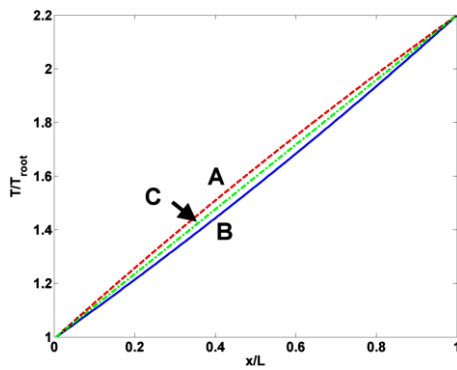


Fig. 4 Temperature distribution of composite blade for three distribution cases of A, B and C

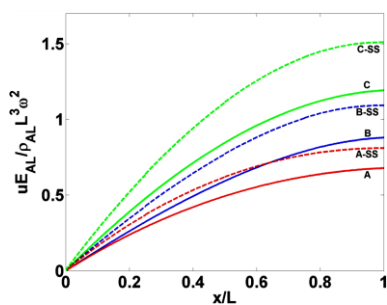


Fig. 5 Initial thermoelastic and steady state (ss) creep longitudinal displacement of composite blade for cases of A, B and C

is satisfied. Maximum elastic and steady creep displacement belongs to pure aluminum (case C) which means the reinforcement has a significant effect on initial elastic and final creep elongation. The minimum elastic and creep displacement belongs to case A indicate thermoelastic and creep distribution of longitudinal deflection of blade for three cases.

In cases A and B the material creep property according to Eqs. (5) and (6) is better than case A therefore higher increasing of steady state creep longitudinal displacement in case C is justified.

Transverse displacement of the blade for three cases A, B and C at zero time and final steady state condition are depicted on Fig. 6. At creep condition absolute transverse displacements are higher than initial elastic at zero time which is expected. However, the reinforcement has not considerable effect on the initial elastic or final creep transverse displacement.

Fig. 7 shows initial thermoelastic and steady state creep longitudinal stresses in three cases A, B and C. the boundary condition at the free tip and fixed root is satisfied. For all three cases stresses are relaxed due to creep. Relaxation for pure aluminum is higher than other cases.

Fig. 8 shows initial thermoelastic and steady state creep shear stresses in three cases A, B and C. Maximum absolute value of shear stresses are located at the root for three cases A, B and C and zero shear stresses are located at the tip which satisfies the boundary condition at the free tip and fixed root. Stress relaxation has occurred throughout the blade the maximum relaxation belongs to pure aluminum at the root (case A).

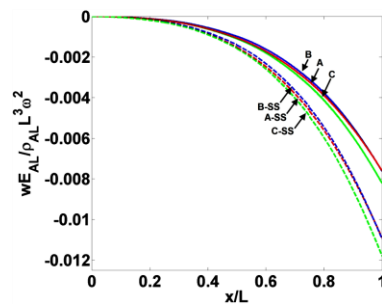


Fig. 6 Initial thermoelastic and steady state (ss) creep longitudinal displacement of composite blade for cases of A, B and C

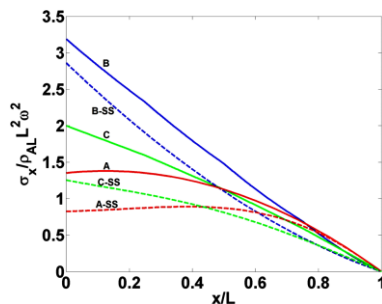


Fig. 7 Initial thermoelastic and steady state (ss) creep longitudinal stress distribution of composite blade for cases of A, B and C

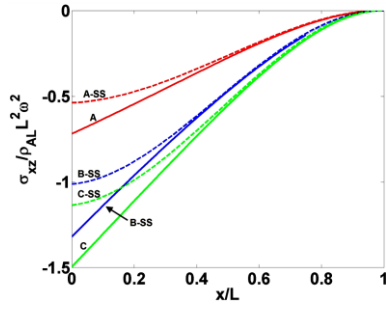


Fig. 8 Initial thermoelastic and steady state (ss) creep shear stress distribution of composite blade for cases of A, B and C

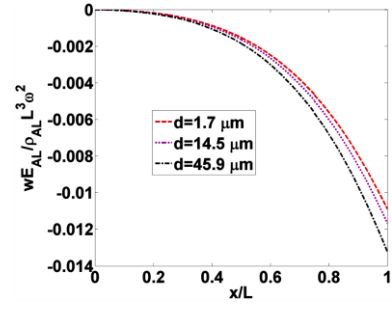


Fig. 11 Steady state creep transverse displacement of composite blade for case A and three different particle size

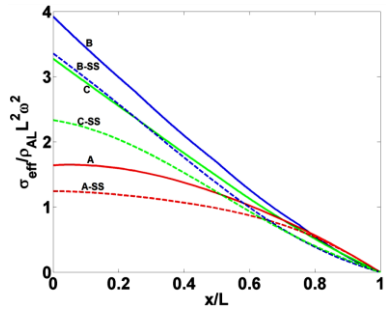


Fig. 9 Initial thermoelastic and steady state (ss) creep effective stress distribution of composite blade for cases of A, B and C

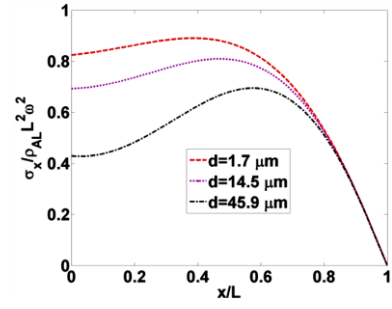


Fig. 12 Steady state creep longitudinal stress of composite blade for case of A and three different particle size

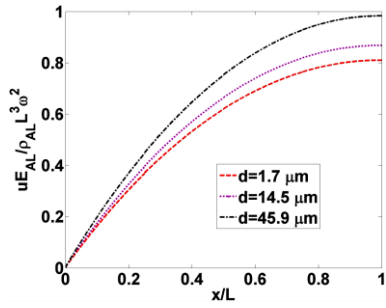


Fig. 10 Steady state creep longitudinal displacement of composite blade for case A and three different particle size

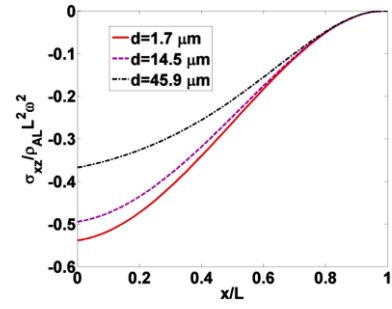


Fig. 13 Steady state creep shear stress of composite blade for case of A and three different particle size

Initial thermoelastic and final steady state creep effective stresses are shown in Fig. 9. These effective stresses satisfy the boundary condition. Stress relaxation has occurred for all three cases. The maximum relaxation has occurred for pure aluminum at the root of the blade. According to Eqs. (5) and (6) the reinforcement particle improves the material creep property therefore higher longitudinal, transverse and effective stress relaxation in case A is expected.

The minimum effective stress distribution belongs to the case A. for this reason this case has been selected for considering the effect of particle size on the steady state creep behavior of the blade.

Figs. 5-11 indicate that reinforcement particle decrease the absolute value of steady state creep displacements and

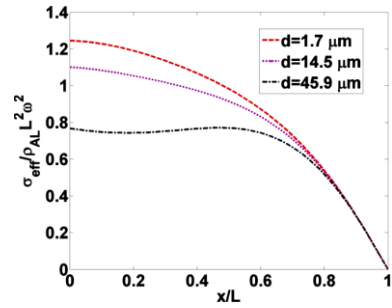


Fig. 14 Steady state creep effective stress of composite blade for case of A and three different particle size

stress relaxations.

The effect of particle size on longitudinal displacement for the selected case A is shown in Fig. 10. Increasing the

particle size is associated with increasing displacement. This is because increasing particle size decreases the creep properties (Pandey *et al.* 1993). The same conclusion can be made for transverse displacement as shown in Fig. 11.

Longitudinal, shear and effective steady state stresses for three different reinforcement particle sizes are shown in Figs. 12-14. Increasing reinforcement particle size is associated with higher relaxation. Maximum relaxation belongs to the  $d = 45.9 \mu\text{m}$  and minimum relaxation is observed for  $d = 1.7 \mu\text{m}$ . Increasing the reinforcement particle size, the maximum value of the longitudinal stress will be shifted to the middle of the blade.

Figs. 10-14 show that, as the particle size increases, the steady state creep absolute value of displacements also increases and stresses decreased.

## 6. Conclusions

In this article, a semi analytical solution has been carried out for steady state creep analysis of a simple turbine blade modelled by a variable thickness cantilever beam. First order shear deformation theory has been employed. Norton's law has been considered for creep constitutive model. Initial thermoelastic stresses and deformations are compared with their steady state creep conditions which clearly show deformations take place due to creep which is associated with creep relaxation. Three cases of reinforcement distribution are studied. It has been found that stress relaxation occurred throughout the blade due to creep. The maximum relaxation belongs to pure aluminum blade at the root. Particle size has also significant effect on steady state creep response of the blade. The maximum relaxation belongs to particle size  $d = 45.9 \mu\text{m}$ .

## Acknowledgments

This work was supported by the University of Kashan under Grant number: 468797.

## References

- Almasi, A. (2015), "Modern guidelines and latest case studies on condition monitoring of rotating equipment", *Austral. J. Mech. Eng.*, **13**(3), 172-186.  
<https://doi.org/10.1080/14484846.2015.1093228>
- Anitescu, C., Atroshchenko, E., Alajlan, N. and Rabczuk, T. (2019), "Artificial neural network methods for the solution of second order boundary value problems", *Comput. Mater. Continua*, **59**, 345-359.
- Arefi, M. and Zenkour, A. (2017a), "Electro-magneto-elastic analysis of a three-layer curved beam", *Smart. Struct. Syst., Int. J.*, **19**(6), 695-703. <https://doi.org/10.12989/sss.2017.19.6.695>
- Arefi, M. and Zenkour, A.M. (2017b), "Size-dependent free vibration and dynamic analyses of piezo-electro-magnetic sandwich nanoplates resting on viscoelastic foundation", *Phys. B: Cond. Matt.*, **521**, 188-197.  
<https://doi.org/10.1016/j.physb.2017.06.066>
- Arefi, M. and Zenkour, A.M. (2017c), "Transient sinusoidal shear deformation formulation of a size-dependent three-layer piezo-magnetic curved nanobeam", *Acta. Mech.*, **228**(10), 3657-3674.  
<https://doi.org/10.1007/s00707-017-1892-6>
- Arefi, M. and Zenkour, A.M. (2018a), "Employing the coupled stress components and surface elasticity for nonlocal solution of wave propagation of a functionally graded piezoelectric Love nanorod model", *J. Intell. Mater. Syst. Struct.*, **28**(17), 2403-2413. <https://doi.org/10.1177/1045389X17689930>
- Arefi, M. and Zenkour, A.M. (2018b), "Size-dependent electro-elastic analysis of a sandwich microbeam based on higher-order sinusoidal shear deformation theory and strain gradient theory", *J. Intell. Mater. Syst. Struct.*, **29**(7), 1394-1406.  
<https://doi.org/10.1177/1045389X17733333>
- Arefi, M., Rahimi, G.H. and Khoshgoftar, M.J. (2012), "Exact solution of a thick walled functionally graded piezoelectric cylinder under mechanical, thermal and electrical loads in the magnetic field", *Smart. Struct. Syst., Int. J.*, **9**(5), 427-439.  
<https://doi.org/10.12989/sss.2012.9.5.427>
- Arefi, M., Faegh, R.K. and Loghman, A. (2016), "The effect of axially variable thermal and mechanical loads on the 2D thermoelastic response of FG cylindrical shell", *J. Thermal Stresses*, **39**(12), 1539-1559.  
<https://doi.org/10.1080/01495739.2016.1217178>
- Arefi, M., Zamani, M.H. and Kiani, M. (2018), "Size-dependent free vibration analysis of three-layered exponentially graded nanoplate with piezomagnetic face-sheets resting on Pasternak's foundation", *J. Intell. Mater. Syst. Struct.*, **29**(5), 774-786.  
<https://doi.org/10.1177/1045389X17721039>
- Chakraborty, A., Gopalakrishnan, S. and Reddy, J.N. (2003), "A new beam finite element for the analysis of functionally graded materials", *Int. J. Mech. Sci.*, **45**(3), 519-539.  
[https://doi.org/10.1016/S0020-7403\(03\)00058-4](https://doi.org/10.1016/S0020-7403(03)00058-4)
- Chau-Dinh, T., Zi, G., Lee, P.-S., Rabczuk, T. and Song, J.-H. (2012), "Phantom-node method for shell models with arbitrary cracks", *Comput. Struct.*, **92-93**, 242-256.  
<https://doi.org/10.1016/j.compstruc.2011.10.021>
- Davoudi Kashkoli, M. and Nejad, M. (2018), "Time-dependent creep analysis and life assessment of 304 L austenitic stainless steel thick pressurized truncated conical shells", *Steel Compos. Struct., Int. J.*, **28**(3), 349-362.  
<https://doi.org/10.12989/scs.2018.28.3.349>
- Duy, H., Van, T. and Noh, H.-C. (2014), Eigen analysis of functionally graded beams with variable cross-section resting on elastic supports and elastic foundation", *Struct. Eng. Mech., Int. J.*, **52**, 1033-1049. <https://doi.org/10.12989/sem.2014.52.5.1033>
- Filippi, M., Carrera, E. and Zenkour, A.M. (2015), "Static analyses of FGM beams by various theories and finite elements", *Compos. Part B: Eng.*, **72**, 1-9.  
<https://doi.org/10.1016/j.compositesb.2014.12.004>
- Giunta, G., Belouettar, S. and Carrera, E. (2010), "Analysis of FGM Beams by Means of Classical and Advanced Theories", *Mech. Adv. Mater. Struct.res*, **17**(8), 622-635.  
<https://doi.org/10.1080/15376494.2010.518930>
- Giunta, G., Crisafulli, D., Belouettar, S. and Carrera, E. (2013), "A thermo-mechanical analysis of functionally graded beams via hierarchical modelling", *Compos. Struct.*, **95**, 676-690.  
<https://doi.org/10.1016/j.compstruc.2012.08.013>
- Golmakaniyoon, S. and Akhlaghi, F. (2016), "Time-dependent creep behavior of Al-SiC functionally graded beams under in-plane thermal loading", *Computat. Mater. Sci.*, **121**(Supplement C), 182-190. <https://doi.org/10.1016/j.commatsci.2016.04.038>
- Guo, H., Zhuang, X. and Rabczuk, T. (2019), "A Deep Collocation Method for the Bending Analysis of Kirchhoff Plate", *Comput. Mater. Continua*, **59**(2), 433-456.
- Gupta, V.K., Singh, S.B., Chandrawat, H.N. and Ray, S. (2004), "Steady state creep and material parameters in a rotating disc of Al-SiC composite", *Eur. J. Mech. - A/Solids*, **23**(2), 335-344. <https://doi.org/10.1016/j.euromechsol.2003.11.005>

- Hamdia, K.M., Ghasemi, H., Zhuang, X., Alajlan, N. and Rabczuk, T. (2018), "Sensitivity and uncertainty analysis for flexoelectric nanostructures", *Comput. Methods Appl. Mech. Eng.*, **337**, 95-109. <https://doi.org/10.1016/j.cma.2018.03.016>
- Hamdia, K.M., Silani, M., Zhuang, X., He, P. and Rabczuk, T. (2017), "Stochastic analysis of the fracture toughness of polymeric nanoparticle composites using polynomial chaos expansions", *Int. J. Fracture*, **206**(2), 215-227. <https://doi.org/10.1007/s10704-017-0210-6>
- Jafari Fesharaki, J., Loghman, A., Yazdipoor, M. and Golabi, S. (2014), "Semi-analytical solution of time-dependent thermomechanical creep behavior of FGM hollow spheres", *Mech. Time-Depend. Mater.*, **18**(1), 41-53. <https://doi.org/10.1007/s11043-013-9212-6>
- Kadoli, R., Akhtar, K. and Ganesan, N. (2008), "Static analysis of functionally graded beams using higher order shear deformation theory", *Appl. Math. Model.*, **32**(12), 2509-2525. <https://doi.org/10.1016/j.apm.2007.09.015>
- Kapania, R.K. and Raciti, S. (1989), "Recent advances in analysis of laminated beams and plates. Part I - Shear effects and buckling", *AIAA Journal*, **27**(7), 923-935. <https://doi.org/10.2514/3.10202>
- Kiani, Y. and Eslami, M.R. (2010), "Thermal buckling analysis of functionally graded material beams", *Int. J. Mech. Mater. Des.*, **6**(3), 229-238. <https://doi.org/10.1007/s10999-010-9132-4>
- Kordkheili, S.A.H. and Naghdabadi, R. (2007), "Thermoelastic analysis of a functionally graded rotating disk", *Compos. Struct.*, **79**(4), 508-516. <https://doi.org/10.1016/j.compstruct.2006.02.010>
- Li, X.F. (2008), "A unified approach for analyzing static and dynamic behaviors of functionally graded Timoshenko and Euler-Bernoulli beams", *J. Sound Vib.*, **318**(4), 1210-1229. <https://doi.org/10.1016/j.jsv.2008.04.056>
- Loghman, A. and Wahab, M.A. (1996), "Creep damage simulation of thick-walled tubes using the  $\Theta$  projection concept", *Int. J. Press. Vessels Pip.*, **67**(1), 105-111. [https://doi.org/10.1016/0308-0161\(94\)00175-8](https://doi.org/10.1016/0308-0161(94)00175-8)
- Loghman, A., Ghorbanpour Arani, A. and Aleayoub, S.M.A. (2011), "Time-dependent creep stress redistribution analysis of thick-walled functionally graded spheres", *Mech. Time-Depend. Mater.*, **15**(4), 353-365. <https://doi.org/10.1007/s11043-011-9147-8>
- Loghman, A., Faegh, R. and Arefi, M. (2017a), "Two dimensional time-dependent creep analysis of a thick-walled FG cylinder based on first order shear deformation theory", *Steel Compos. Struct., Int. J.*, **26**(5), 533-547. <https://doi.org/10.12989/scs.2018.26.5.533>
- Loghman, A., Hammami, M. and Loghman, E. (2017b), "Effect of the silicon-carbide micro- and nanoparticle size on the thermoelastic and time-dependent creep response of a rotating Al-SiC composite cylinder", *J. Appl. Mech. Tech. Phys.*, **58**(3), 443-453. <https://doi.org/10.1134/S0021894417030099>
- Mendelson, A. (1968), *Plasticity Theory and Applications*, The Macmillan Company.
- Mirsky, I. (1959), "Axially symmetric motions of thick cylindrical shells", **25**, 97-102.
- Nguyen, T.-K., Vo, T.P. and Thai, H.-T. (2013), "Static and free vibration of axially loaded functionally graded beams based on the first-order shear deformation theory", *Compos. Part B: Eng.*, **55**, 147-157. <https://doi.org/10.1016/j.compositesb.2013.06.011>
- Niknam, H., Fallah, A. and Aghdam, M.M. (2014), "Nonlinear bending of functionally graded tapered beams subjected to thermal and mechanical loading", *Int. J. Non-Linear Mech.*, **65**(Supplement C), 141-147. <https://doi.org/10.1016/j.ijnonlinmec.2014.05.011>
- Oh, Y. and Yoo, H.H. (2016), "Vibration analysis of rotating pretwisted tapered blades made of functionally graded materials", *Int. J. Mech. Sci.*, **119**(Supplement C), 68-79. <https://doi.org/10.1016/j.ijmecsci.2016.10.002>
- Pandey, A.B., Mishra, R.S. and Mahajan, Y.R. (1993), "Creep fracture in Al-SiC metal-matrix composites", *J. Mater. Sci.*, **28**(11), 2943-2949. <https://doi.org/10.1007/BF00354697>
- Rao, J.S. and Vyas, N.S. (1996), "Determination of blade stresses under constant speed and transient conditions with nonlinear damping", *J. Eng. Gas Turbines Power*, **118**(2), 424-433. <https://doi.org/10.1115/1.2816607>
- Roy, P.A. and Meguid, S.A. (2018), "Analytical modeling of the coupled nonlinear free vibration response of a rotating blade in a gas turbine engine", *Acta Mechanica*, **229**(8), 3355-3373. <https://doi.org/10.1007/s00707-018-2165-8>
- Sankar, B.V. (2001), "An elasticity solution for functionally graded beams", *Compos. Sci. Technol.*, **61**(5), 689-696. [https://doi.org/10.1016/S0266-3538\(01\)00007-0](https://doi.org/10.1016/S0266-3538(01)00007-0)
- Sankar, B.V. and Tzeng, J.T. (2002), "Thermal stresses in functionally graded beams", *AIAA Journal*, **40**(6), 1228-1232. <https://doi.org/10.2514/2.1775>
- Sapountzakis, E.J. and Panagos, D.G. (2008), "Shear deformation effect in non-linear analysis of composite beams of variable cross section", *Int. J. Non-Linear Mech.*, **43**(7), 660-682. <https://doi.org/10.1016/j.ijnonlinmec.2008.03.005>
- Shi, G., Lam, K.Y. and Tay, T.E. (1998), "On efficient finite element modeling of composite beams and plates using higher-order theories and an accurate composite beam element", *Compos. Struct.*, **41**(2), 159-165. [https://doi.org/10.1016/S0263-8223\(98\)00050-6](https://doi.org/10.1016/S0263-8223(98)00050-6)
- Vu-Bac, N., Lahmer, T., Zhuang, X., Nguyen-Thoi, T. and Rabczuk, T. (2016), "A software framework for probabilistic sensitivity analysis for computationally expensive models", *Adv. Eng. Software*, **100**, 19-31. <https://doi.org/10.1016/j.advengsoft.2016.06.005>
- Xu, Y. and Zhou, D. (2012), "Two-dimensional thermoelastic analysis of beams with variable thickness subjected to thermo-mechanical loads", *Appl. Math. Model.*, **36**(12), 5818-5829. <https://doi.org/10.1016/j.apm.2012.01.048>
- Zappino, E., Viglietti, A. and Carrera, E. (2018), "Analysis of tapered composite structures using a refined beam theory", *Compos. Struct.*, **183**, 42-52. <https://doi.org/10.1016/j.compstruct.2017.01.009>

CC